

Estimation of Channel Temporal Auto-Correlation and Coherence Time based on Propagation Paths

Xuefeng Yin¹, Junhe Zhou¹, Byung-Jae Kwak² and Hyun Kyu Chung²

¹School of Electronics and Information Engineering, Tongji University, Shanghai, China

²Electronics and Telecommunications Research Institute, Daejeon, Republic of Korea

Email: {yinxuefeng, jhzhou}@tongji.edu.cn, {bjkwak, hkchung}@etri.re.kr

Abstract—In this contribution, we investigate the applicability of using multiple propagation paths to estimate the temporal auto-correlation function and the coherence time of wireless propagation channels. The Space-Alternating Generalized Expectation-maximization (SAGE) algorithm is applied for extracting the paths from measurement data. It is found that the channel auto-correlation function and coherence time computed based on the path parameters are biased. A simple method is proposed for correction of the biases. Experimental investigations are conducted to evaluate the effectiveness of the method.

Index Terms—Wireless channel, propagation path, Doppler frequency, channel temporal auto-correlation, channel coherence time and the SAGE algorithm.

I. INTRODUCTION

The characteristics of propagation channels have significant impact on the performance of wireless communication systems [1]. The channel variability in time can be characterized by the temporal auto-correlation function (ACF) of the channel impulse response (CIR) and the so-called coherence time of the channel [2]. Fully understanding of these characteristics are of great importance for the design of wireless communication systems and performance optimization for the systems.

The temporal ACF and coherence time of a channel are usually estimated using the observed CIRs in measurements. The CIRs can be calculated by applying two methods, i.e. *i*) correlation of the received signal with transmitted signal, and *ii*) reconstruction using the estimates of the parameters of a generic propagation model. In the latter method, the specular-path model is usually used under the assumption that the CIR consists of the contributions of planar waves propagating along multipath. The parameters of the paths can be estimated from the received signals by using high-resolution estimation algorithms, such as the Space-Alternating Generalized Expectation-maximization (SAGE) algorithm [3], the Richter Maximum-likelihood (RiMAX) algorithm [4] and the Estimation of Signal Parameters via Rotational Invariance Techniques

This work was jointly supported by the IT R&D program of MKE/KCC/KEIT. [KI002060, Wideband Wireless Channel Modeling based on IMT-Advanced], the project of the Science and Technology Commission of Shanghai Municipality [10ZR1432700, Multidimensional power spectrum characterization and modeling for wide-band propagation channels], the China Important National Science and Technology Specific Project [20090072120015, Research on Channel Measurement and Modeling for IMT-Advanced System], the China Education Ministry “New-teacher” Project [20090072120015, Time-Variant Channel Characterization, Parameter Estimation and Modeling] and the 985 program project of Tongji University [Wireless channel analysis and testing for the 4th generation mobile communications].

(ESPRIT) [5]. As the constellation of the paths are closely related to the geometry of the scattering environments, the method *ii*) is usually referred to as the “geometric approach”. Theoretically, provided the CIRs are precisely represented by multipath components, the two methods yield the same estimates for the channel temporal ACF and channel coherence time.

Validation of using multipath components to represent the channel characteristics in space and frequency has been conducted experimentally in [6]. As far as we are concerned, similar investigations have not been performed in the time domain. Considering that the multipath propagation models, such as the 3GPP spatial-channel models (SCM) [7] and the WINNER models [8], have been widely used for channel simulation, it is important to evaluate the effectiveness of applying multipath to predict channel temporal behavior, i.e. the temporal ACF and channel coherence time of the channel.

In this contribution, we analyze the consistency of the channel temporal ACF estimator based on multipath, and propose a method to mitigate the bias in the ACF estimator. Experimental investigations are conducted to assess the applicability of the method in reality.

The paper is organized as follows. Section II describes the CIR and the conventional method for computing the temporal ACF. Section III introduces the high-resolution parameter estimation method based on the SAGE algorithm. In Section IV, the estimator of the temporal ACF based on multipath is described. In Section V, the experimental results in two indoor scenarios are presented. Conclusion remarks are given in Section VI.

II. SIGNAL MODEL

Following the nomenclature in [9], we model the impulse response $h(\tau, \nu)$ of a propagation channel in delay and Doppler frequency as a superposition of L specular path components, i.e.

$$h(\tau, \nu) = \sum_{\ell=1}^L \alpha_{\ell} \delta(\tau - \tau_{\ell}) \delta(\nu - \nu_{\ell}), \quad (1)$$

where α_{ℓ} , τ_{ℓ} and ν_{ℓ} denote respectively the complex attenuation, the delay and the Doppler frequency of the ℓ th path. Under the assumption that α_{ℓ} , $\ell = 1, \dots, L$ are uncorrelated stochastic processes, i.e. $E[\alpha_{\ell} \alpha_{\ell'}^*] = p_{\ell} \delta_{\ell \ell'}$ with $(\cdot)^*$ representing the complex conjugate of the given argument, $p_{\ell} =$

$E[|\alpha_\ell|^2]$ being the power of the ℓ th path component, and $\delta_{\ell\ell'}$ denoting a dirac delta function, the delay-Doppler frequency power spectrum $p(\tau, \nu)$ of the channel can be calculated as

$$p(\tau, \nu) = E[h(\tau, \nu)h(\tau, \nu)^*] \\ = \sum_{\ell=1}^L p_\ell \delta(\tau - \tau_\ell) \delta(\nu - \nu_\ell). \quad (2)$$

The temporal observations of a wideband channel $h(\tau, t)$ is calculated as

$$h(\tau, t) = \int_{-\infty}^{+\infty} h(\tau, \nu) \exp\{j2\pi\nu t\} d\nu. \quad (3)$$

The temporal ACF $C_h(\Delta t)$ of the channel is defined as [2]

$$C_h(\Delta t) \doteq \frac{E_{t,\tau}[h(\tau, t)h(\tau, t + \Delta t)^*]}{E_{t,\tau}[|h(\tau, t)|^2]} \\ = \sum_{\ell=1}^L \frac{p_\ell}{P} \exp\{-j2\pi\nu_\ell \Delta t\} \text{ with } P = \sum_{\ell=1}^L p_\ell, \quad (4)$$

where $E_{t,\tau}[\cdot]$ represents the expectation of the given argument over time and delay. The coherence time T_c of the channel can be obtained from $C_h(\Delta t)$. In this contribution, we use the method proposed in [2] to compute T_c , i.e.

$$T_c \approx \frac{2\pi}{5\sigma} \quad (5)$$

where σ is the standard deviation of a Gaussian probability density function fitted to $C_h(\Delta t)$.

III. THE SAGE ALGORITHM

The SAGE algorithm is an iterative algorithm which returns parameter estimates that approximate the values obtained using the maximum likelihood method. In this contribution, the SAGE algorithm is used to estimate the delays, Doppler frequencies and complex attenuations of L' path components. The value of L' is set heuristically to a large number so that the extracted paths can represent the dominant components in the channel response [10]. Experimental results show that a propagation channel usually consists of a certain number of well-separated path components and a tremendous amount of closely-spaced path components [11]. The closely-spaced path components are called dense-multipath components [11] or dispersive components [12], or clusters [13]. In the cases where the channel contains dense-multipath components, as in many micro-cell and indoor scenarios, under the practical limit of computational complexity the SAGE algorithm is applicable for extracting a portion of the true paths. This implies that a significant amount of paths are left unestimated, and thus, the inequality $L' \ll L$ is reasonable in such cases.

We use $\Theta = (\theta_1, \theta_2, \dots, \theta_{L'})$ to denote the unknown parameters for estimation, where $\theta_\ell = (\tau_\ell, \nu_\ell, \alpha_\ell)$, $\ell \in [1, \dots, L']$ representing the parameters associated with the ℓ th path. In the i th iteration of the SAGE algorithm, the estimates of the parameters in θ_ℓ , $\ell = \text{mod}(i, L') + 1$ are updated. The admissible-hidden data for estimation of θ_ℓ reads

$$X_\ell(t, \tau) = \alpha_\ell s(\tau - \tau_\ell) \exp\{j2\pi\nu_\ell t\} + w(t, \tau), \quad (6)$$

where $s(\tau)$ is the transmitted signal, $w(t, \tau)$ denotes the circular-symmetric white Gaussian noise with variance σ_w^2 .

Each iteration of the SAGE algorithm consists of two steps, namely the expectation (E-) step and the maximization (M-) step. In the E-step, an objective function

$$Q(\theta_\ell | \hat{\Theta}^{[i-1]}) \doteq E[\Lambda(\theta_\ell; X_\ell) | Y(t) = y(t), \hat{\Theta}^{[i-1]}] \quad (7)$$

is computed, where $\hat{\Theta}^{[i-1]}$ is the estimate of Θ at the $i-1$ th iteration, $\Lambda(\theta_\ell; X_\ell)$ represents the loglikelihood function of θ_ℓ , $Y(t)$ denotes the received signal, and $y(t)$ is an observation of $Y(t)$. In the M-step, the parameter estimates are obtained as

$$\hat{\theta}_\ell^{[i]} = \arg \max_{\theta_\ell} \{Q(\theta_\ell | \hat{\Theta}^{[i-1]})\}. \quad (8)$$

In the initialization step of the SAGE algorithm, we use a successive interference cancellation method to obtain the initial estimates $\hat{\theta}_\ell^{[0]}$, $\ell = 1, \dots, L'$. The reader is referred to [3] for the details of the initialization method.

IV. TEMPORAL ACF ESTIMATOR BASED ON MULTIPATH

Using the parameter estimates $\hat{\Theta}$ returned by the SAGE algorithm, the channel temporal ACF can be calculated as

$$\hat{C}_h(\Delta t) = \sum_{\ell=1}^{L'} \frac{\hat{p}_\ell}{P'} \exp\{-j2\pi\hat{\nu}_\ell \Delta t\} \text{ with } P' = \sum_{\ell=1}^{L'} \hat{p}_\ell. \quad (9)$$

As L' is considered to be less than L , the true ACF $C_h(\Delta t)$ in (4) can be rewritten as

$$C_h(\Delta t) = \sum_{\ell=1}^{L'} \frac{p_\ell}{P} \exp\{-j2\pi\nu_\ell \Delta t\} \\ + \sum_{\ell=L'+1}^L \frac{p_\ell}{P} \exp\{-j2\pi\nu_\ell \Delta t\}. \quad (10)$$

Assuming that $\hat{\theta}_\ell \approx \theta_\ell$ for $\ell < L'$, it can be shown that

$$C_h(\Delta t) \approx \hat{C}_h(\Delta t) P^{-1} P' + n(\Delta t) \quad (11)$$

$$\Rightarrow \hat{C}_h(\Delta t) \approx P/P' (C_h(\Delta t) - n(\Delta t)) \quad (12)$$

with $n(\Delta t) = P^{-1} \sum_{\ell=L'+1}^L p_\ell \exp\{-j2\pi\nu_\ell \Delta t\}$. According to Section III, when a channel contains dense-multipath components, the inequality $L \ll L'$ holds. By applying the central limit theorem, it can be shown that $n(\Delta t)$ is a Gaussian random variable with zero mean. Taking the expectation of both sides of (12), we obtain

$$E[\hat{C}_h(\Delta t)] = C_h(\Delta t) P/P'. \quad (13)$$

The bias of the estimator $\hat{C}_h(\Delta t)$ is then calculated as

$$\text{Bias}[\hat{C}_h(\Delta t)] = C_h(\Delta t) \frac{P - P'}{P}. \quad (14)$$

From (14), we can see that the estimator $\hat{C}_h(\Delta t)$ is unbiased if and only if $L' = L$ and $\hat{\theta}_\ell = \theta_\ell$ for $\ell = 1, \dots, L$. Furthermore, from (14) we see that the bias of $\hat{C}_h(\Delta t)$ can be removed

by multiplying $\hat{C}_h(\Delta t)$ in (9) with a factor P'/P . Thus, a corrected estimator $\check{C}_h(\Delta t)$ can be calculated as

$$\begin{aligned} \check{C}_h(\Delta t) &= P'/P \hat{C}_h(\Delta t) \\ &= \sum_{\ell=1}^{L'} \frac{\hat{p}_\ell}{P} \exp\{-j2\pi\hat{\nu}_\ell\Delta t\}, \end{aligned} \quad (15)$$

where the total power P of the true paths can be estimated by the average of the energy of the CIRs observed at different t , i.e. $\hat{P} = \langle \int_0^T |h(t, \tau)|^2 d\tau \rangle$, with T denoting the time span of one observation. Notice that this unbiased estimator $\check{C}_h(\Delta t)$ is indeed the well-known unbiased estimation technique for the second-moment of random processes applied in the context considered in this paper [14].

We compute the channel coherence time T_c by applying (5) as described in Section II. It can be shown that when T_c is estimated using $\hat{C}_h(\Delta t)$, the estimator \hat{T}_c of T_c is biased with $\text{Bias}[\hat{T}_c] \approx T_c(1 - \sqrt{P'/P})$. However, this bias can be suppressed when $\hat{C}_h(\Delta t)$ is replaced by the unbiased estimator $\check{C}_h(\Delta t)$.

V. EXPERIMENTAL INVESTIGATION

In this section, channel measurement data are used to validate the accuracy of the proposed method in estimating the channel temporal ACF and the channel coherence time. Our original idea is to compare the estimates with their measured counterparts. However, as the channel is measured with low repetition rate, we are unable to compute $C_h(\Delta t)$ with refined grids in Δt . In such a case, the ‘‘true’’ $C_h(\Delta t)$ is calculated via Fourier transformation of the empirical channel Doppler frequency spectrum.

A. Measurement settings

The measurement data were collected in a campaign organized by Technology University of Vienna and Elektrotbit in Oulu University, using the wideband MIMO channel sounder - Propsound [8]. The Tx and Rx of the sounder were equipped with a similar 50-element antenna array. The bandwidth of the Rx was 200 MHz. The so-called subchannels, i.e. the channels between individual pairs of the Tx and Rx antennas, were measured sequentially using two switches, located in the Tx and the Rx respectively. The switches operated in a time-division-multiplexing (TDM) mode consisting of cycles and bursts. Here, a burst contains multiple cycles. A cycle is referred to as the duration within which all subchannels are measured once. Each burst consists of 4 cycles. The interval between the starts of two consecutive cycles and two consecutive bursts equals $T_{\text{cyc}} = 16.8$ ms and 268.8 ms respectively.

Two scenarios are considered for the evaluation. Scenario I is referred to as the measurement performed in a narrow corridor between office rooms. Scenario II is the measurement conducted in a wide corridor with people walking. The location of the Rx was fixed in both scenarios, while the Tx moved at constant speed of 0.5 m/s. We assume that the parameters, i.e. the delays, Doppler frequencies and complex attenuations of propagation paths are constant within

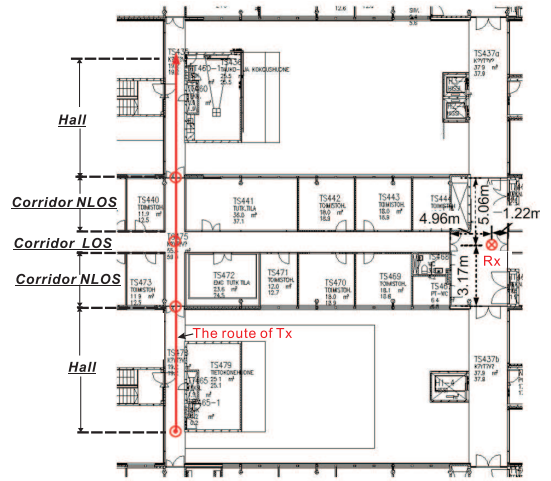


Fig. 1. The map of the premises for Scenario I measurement. When the Tx moved, the propagation scenario changed from ‘‘hall’’ to ‘‘corridor NLOS’’, ‘‘corridor LOS’’, then ‘‘corridor NLOS’’ and finally back to ‘‘hall’’.

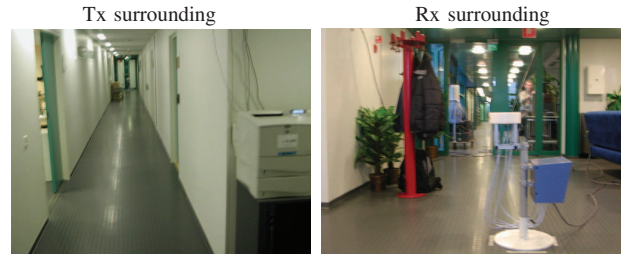


Fig. 2. Photographs of the surrounding of the Tx and Rx in Scenario I.

the 4 cycles in each burst. The SAGE algorithm is used to estimate the parameters of L' paths based on the received signal. The Doppler frequency was estimated within the range $[-1/(2T_{\text{cyc}}), 1/(2T_{\text{cyc}})] = [-29.7, 29.7]$ Hz.

B. Scenario I

Fig. 1 illustrates the map of the environment where the measurement was conducted. During the measurement, the Tx moved along a straight route in a corridor from the bottom to the top of the map. It can be seen from Fig. 1 that when the Tx was moving, the propagation scenario evolved gradually from an open hall to a corridor with non-line-of-sight (NLOS), then to a line-of-sight (LOS) case when the Tx arrived at the middle of the measurement route. When the Tx moved continuously, the propagation scenario changed from LOS to NLOS corridor, and back to open hall when the Tx reached the route end. Fig. 2 shows the photographs of the surroundings of the Tx and Rx when the measurement started.

Fig. 3 illustrates the estimates of the Doppler frequencies of 30 specular paths versus the burst indices. The colors of the spots code the amplitude of the paths in dB. We can observe that when the Tx moves, the power Doppler frequency spectrum in terms of discrete paths exhibits different profiles. The Doppler spread is large when the Tx was in the hall, and decreases when the Tx was approaching the LOS in the corridor.

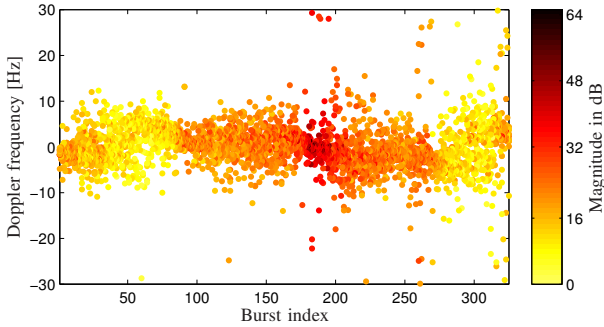


Fig. 3. Doppler frequency estimates of specular paths for 100 bursts in the scenario depicted in Fig. 1, with $L = 30$ and dynamic range equal to 40 dB.

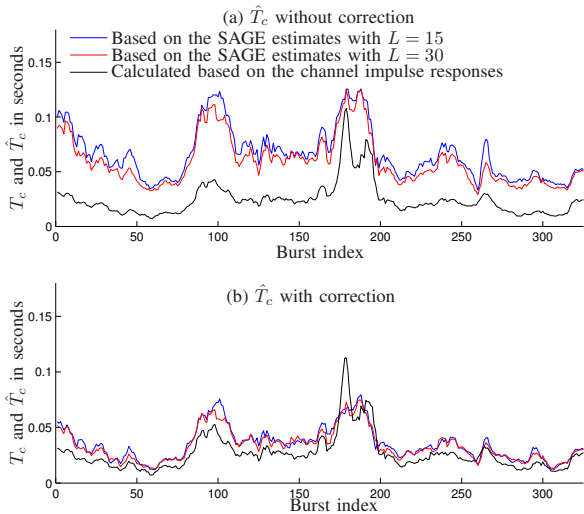


Fig. 4. Comparison between the measured coherence time T_c and the calculated coherence time \hat{T}_c without correction (a) and \check{T}_c with correction (b).

From the estimates shown in Fig. 3, we calculate the estimate of the temporal ACFs and the coherence time of the channel. Fig. 4 (a) depicts the measured T_c and calculated \hat{T}_c based on $\hat{C}_h(\Delta t)$ in (13). Two values of \hat{T}_c are presented which are obtained by using the estimates of $L' = 15, 30$ paths respectively. The following phenomena are observed from Fig. 4. First, without the correction suggested in (13), \hat{T}_c is always larger than the measured T_c regardless of L . This is consistent with the theoretical result shown in Section IV. Second, the variations of \hat{T}_c and T_c with respect to the burst index are similar. These variations are also correlated with the changes of the Doppler frequency spectra dependent on the exact propagation scenarios. Furthermore, when a large L' is selected, the deviation between \hat{T}_c and T_c does not decrease significantly. This indicates that without performing any correction, the specular path models indeed fails to reproduce the temporal ACF and the coherence time of a channel.

Fig. 4 (b) depicts the calculated coherence time \check{T}_c that are obtained by applying the corrected ACF estimator in (13). It can be observed that the deviation between \check{T}_c and T_c decreases significantly. This shows that the estimation of T_c

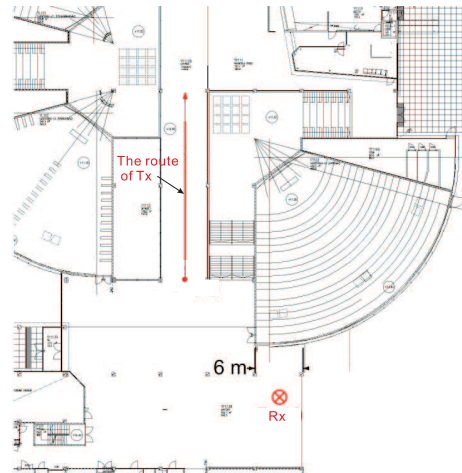


Fig. 5. The map of the environment where Scenario II measurement was conducted.

can be improved by multiplying \hat{T}_c with the ratio between the sum of the powers of all estimated paths and the total energy of the channel response. It is important to consider this ratio when simulating the temporal characteristics of propagation channels using geometry-based models.

From Fig. 4 (b) we also observe that for the cycles around 180, i.e. when the Tx and Rx have LOS connection, \hat{T}_c is larger than T_c . We postulate that this overestimation effect is because the number of paths to be estimated, i.e. $L' = 30$ is larger than the true path number L in the LOS scenario. The artifact paths returned by the SAGE algorithm lead to the incorrect estimate of the ACF and the coherent time. This observation shows that the unbiased estimator $\check{C}_h(\Delta t)$ is applicable for the cases with $L' < L$ e.g. in rich-scattering scenarios.

C. Scenario II

The environment where Scenario II measurement was conducted is depicted in Fig. 5. During the measurement, the Tx was moving in a wide corridor along a route marked in Fig. 5. People were walking in the corridor constantly. Fig. 6 depicts the photographs of the surroundings of the Tx and Rx when the measurement began.

Fig. 7 depicts the Doppler frequency estimates of $L' = 50$ propagation paths obtained using the SAGE algorithm. We observe that the estimated power Doppler frequency spectrum in terms of discrete paths exhibit a “tub” shape as derived based on the Jakes’ model [15]. The borders of the tub-shaped spectrum are located in respectively, the positive and negative part of the Doppler frequency axis. The spread of the power Doppler frequency spectrum increases gradually when the Tx moves.

Fig. 8 (a) depicts the coherence time T_c and the non-corrected \hat{T}_c which are calculated using the estimates of path parameters obtained from the SAGE algorithm for $L' \in [15, 20, 30, 50]$. We observe similar phenomena as shown in Scenario I, i.e. the non-corrected \hat{T}_c is larger than T_c , and the distance between \hat{T}_c and T_c does not vary significantly for different L . Fig. 8 (b) compares the corrected \check{T}_c and T_c . It can be observed that the deviation between \check{T}_c and T_c is

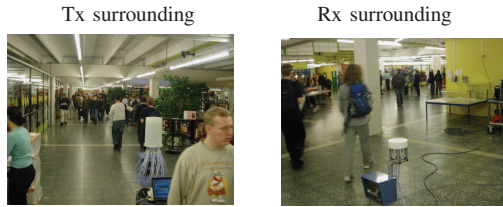


Fig. 6. Photographs of the surrounding of the Tx and Rx in Scenario II.

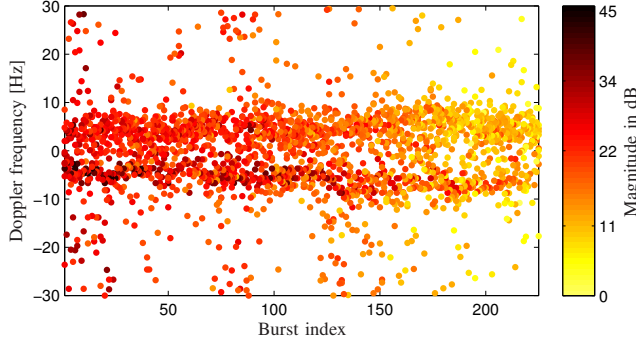


Fig. 7. Doppler frequency estimates of specular paths for 100 bursts in Scenario II, with $L = 50$.

significantly reduced. We also observe that the large deviations even after applying the correction. This can be due to the fact that the number of paths set in the SAGE algorithm is not large enough, so that the paths estimated by the SAGE algorithm cover only portion of the channel response. The problem may be solved by allocating the paths to a certain number of delay bins which are predetermined in such a way that the estimates returned represent the overall profile of the propagation channel.

VI. CONCLUSIONS

In this contribution, we proposed a simple method for enhancing the accuracy of applying multiple propagation paths to the reconstruction of the temporal auto-correlation characteristics of channels. We first showed that the estimates of the temporal auto-correlation of the channel and coherence time computed based on the path parameters are inconsistent with their true values. In the proposed method, a correction factor is introduced which is calculated based on the power estimates of paths, and used to mitigate the estimation errors. Experimental results showed that by using the proposed method, the deviation between the calculated coherence time and the measured value was reduced significantly. These results are useful for accurate simulation of time-variant channels using the geometry-based stochastic channel models.

VII. ACKNOWLEDGEMENT

The authors would like to acknowledge the Elektrobitt company, Finland for kindly providing the measurement data.

REFERENCES

[1] P. Kyritsi, D. Cox, R. Valenzuela, and P. Wolniansky, "Correlation analysis based on mimo channel measurements in an indoor environment," *Selected Areas in Communications, IEEE Journal on*, vol. 21, no. 5, pp. 713–720, June 2003.

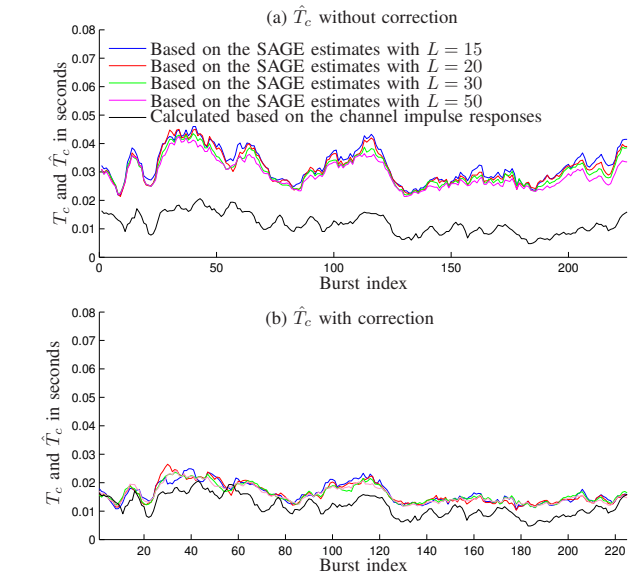


Fig. 8. Comparison between the measured coherence time T_c and the calculated coherence time \hat{T}_c without correction (a) and \hat{T}_c with correction (b).

[2] G. D. Durgin, *Space-Time Wireless Channels*. Upper Saddle River, NJ: Pearson Education, 2003.

[3] X. Yin, B. Fleury, P. Jourdan, and A. Stucki, "Polarization estimation of individual propagation paths using the sage algorithm," *Personal, Indoor and Mobile Radio Communications, 2003. PIMRC 2003. 14th IEEE Proceedings on*, vol. 2, pp. 1795–1799, Sept. 2003.

[4] A. Richter and R. S. Thoma, "Joint maximum likelihood estimation of specular paths and distributed diffuse scattering," in *Proceedings of the IEEE 61st Vehicular Technology Conference (VTC-Spring)*, vol. 1, no. 1, Stockholm, May 2005, pp. 11–15.

[5] R. Roy and T. Kailath, "ESPRIT - estimation of signal parameters via rotational invariance techniques," *IEEE Transactions on Acoustics, Speech, and Signal Processing*, vol. 37, no. 7, pp. 984–995, July 1989.

[6] J. Medbo, M. Riback, and J. Berg, "Validation of 3GPP spatial channel model including WINNER wideband extension using measurements," in *Proceedings of IEEE 64th Vehicular Technology Conference, (VTC2006-Fall)*, Montréal, Canada, September, 25–28 2006.

[7] 3GPP, "Tr 25.996 spatial channel model for multiple input multiple output (mimo) simulations, v6.1.0," Tech. Rep., 2003–09.

[8] P. Kyösti, J. Meinilä, L. Hentilä, X. Zhao, T. Jämsä, C. Schneider, M. Narandzić, M. Milojević, A. Hong, J. Ylitalo, V.-M. Holappa, M. Alatossava, R. Bultitude, Y. de Jong, and T. Rautiainen, "WINNER II Channel Models D1.1.2 V1.1," no. IST-4-027756 WINNER II, D1.1.2 V1.1, 11 2007.

[9] B. H. Fleury, "First- and second-order characterization of direction dispersion and space selectivity in the radio channel," *IEEE Transactions on Information Theory*, no. 6, pp. 2027–2044, Sept. 2000.

[10] B. H. Fleury, M. Tschudin, R. Heddergott, D. Dahlhaus, and K. L. Pedersen, "Channel parameter estimation in mobile radio environments using the SAGE algorithm," *IEEE Journal on Selected Areas in Communications*, vol. 17(3), no. 3, pp. 434–450, Mar. 1999.

[11] A. Richter and R. S. Thomä, "Parametric modelling and estimation of distributed diffuse scattering components of radio channels," COST273, Tech. Rep. TD-03-198, 2003.

[12] X. Yin, T. Pedersen, N. Czink, and B. Fleury, "Parametric characterization and estimation of bi-azimuth and delay dispersion of individual path components," Nov. 2006, pp. 1–8.

[13] N. Czink, X. Yin, H. Özcelik, M. Herdin, E. Bonek, and B. Fleury, "Cluster Characteristics in a MIMO Indoor Propagation Environment," *Wireless Communications, IEEE Transactions on*, vol. 6, no. 4, pp. 1465–1475, 2007.

[14] K. S. Shanmugan and A. M. Breipohl, *Random Singals: Detection, Estimation and Data Analysis*. John Wiley & Sons, 1988.

[15] W. C. Jakes, *Microwave Mobile Communications*. New York: New York: IEEE Press, 1974.